crystals

MDPI

*Article*

# Mn-Doped Alumina Pink Pigment Prepared by Spray Drying Technique

**Stanislav Kurajica *, Katarina Mužina and Ana Petračić †**

Faculty of Chemical Engineering and Technology, University of Zagreb, 10000 Zagreb, Croatia; kmuzina@fkit.unizg.hr (K.M.)

* Correspondence: stankok@fkit.unizg.hr

† S. K and K. M. dedicate this paper to the memory of our colleague and friend Ana Petračić who passed away far too soon.

**Abstract**

The synthesis of a manganese-doped α-alumina pink pigment via the spray drying technique was explored. Three samples were prepared: pure α-alumina and two doped variants, where 3 and 6% of aluminum were substituted with manganese. The materials were analyzed using differential thermal and thermogravimetric analysis, X-ray diffraction, scanning electron microscopy, energy-dispersive X-ray spectroscopy, and UV-Vis reflectance spectroscopy. Calcination at 1000 °C resulted in α-alumina with minor traces of hausmannite. The incorporation of manganese into the α-alumina crystal lattice was confirmed through lattice constant calculations and EDS. Higher-temperature treatments eliminated hausmannite but led to the formation of manganese aluminate. Washing the samples with hot concentrated hydrochloric acid removed hausmannite, unveiling the desired pink coloration.

**Keywords:** alumina; doping; manganese; pigment; spray drying

## 1. Introduction

Aluminum oxide, $Al_2O_3$, commonly called alumina, can appear in several polymorphic modifications, of which the alpha phase is the most stable. Thanks to its favorable properties, alumina is a highly versatile material used in a wide range of technological applications [1,2]. Research on doped alumina is extensive, as introducing different elements into its crystal structure, by substituting host metal ions with guest metal species, can significantly alter its physical and chemical characteristics [3–5]. One of the most intriguing effects of doping is the modification of optical properties, particularly color. When manganese is introduced into alumina, it imparts a distinctive pink hue, making it valuable as an allochromatic pigment for ceramics [6–9] and prosthetic dentistry [9]. Additionally, manganese doping enhances luminescent properties [10] and can even improve the abrasive properties of alumina [11]. Alumina-based pigments are particularly prized for their ability to endure extreme temperatures and chemical exposure [12], making them ideal for ceramic glazes. Therefore, manganese-doped alumina is investigated in an effort to increase the pool of ceramic pigments with high thermal and chemical stability [3]. The solubility of manganese in alumina is limited, while the amount of dopant which can be incorporated into the crystal structure, i.e., the amount of manganese that can be added to the system without the appearance of secondary phases, largely depends on the synthesis method. The most important factor is the homogeneity of the precursor's mixture [13]. The process is also strongly influenced by temperature [4].

Check for updates

Academic Editors: Silvana Moris López and Jiamin Wu

Received: 15 March 2026
Revised: 17 April 2026
Accepted: 30 April 2026
Published: 5 May 2026

**Copyright:** © 2026 by the authors. Licensee MDPI, Basel, Switzerland. This article is an open access article distributed under the terms and conditions of the Creative Commons Attribution (CC BY) license.

The traditional solid-state process for the preparation of doped alumina consists of mixing fine alumina powder with a small amount of manganese oxide, followed by high-temperature calcination under a high-vacuum or hydrogen atmosphere for an extended period [14]. While effective, this method has significant drawbacks, including the need for extremely high calcination temperatures and the incomplete reaction of precursors. To mitigate these issues, flux agents are often added to the reaction mixture, but this violates the purity of the final product [8]. Therefore, attempts were made to prepare manganese-doped alumina using different synthesis approaches enabling the homogeneous distribution of dopants. Some of these approaches are: combustion synthesis [8], immersion in salt solutions [10], hydrothermal synthesis [15], sol–gel [16], the pyrolysis of aerosols [6,7], the polymeric precursor method [9], coprecipitation [17] etc. Each of these techniques offers distinct advantages, such as improved dopant dispersion, lower processing temperatures, and better control over particle morphology. Spray drying is widely recognized as an efficient and adaptable technique for producing high-purity ceramic powders [18,19]. This method transforms a liquid suspension or solution, whether water- or organic-based, into a dry powder by atomizing it into a stream of hot air. As the solvent rapidly evaporates, solid particles form and are subsequently separated from the air using a cyclone and collected in a designated container [19,20]. The process is not only fast and continuous but also cost-effective, enabling the production of high-purity particles with precisely controlled sizes [19,21]. The primary benefit of using spray drying for pigment preparation is the ability to produce highly homogeneous pure powders [22]. However, there is limited information on how thermal treatment affects phase evolution in this system.

This study aimed to investigate the synthesis of a manganese-doped alumina pink pigment utilizing the spray drying method with the use of aluminum chelate as feedstock. Additionally, the effects of manganese concentration and thermal treatment temperature on the phase composition (secondary phase appearance) and color properties of the prepared samples were systematically examined.

## 2. Materials and Methods

Three samples were prepared with cation substitution percentages of 0, 3 and 6%, i.e., with nominal composition $Al_{2-X}Mn_{2X}O_3$, where x = 0, 0.03 and 0.06, so the samples were named M0, M3 and M6, respectively. The details of the synthesis have been reported elsewhere [23]. Briefly, raw materials, aluminum nitrate nonahydrate (Kemika, Zagreb, Croatia, 98.5%) and manganese nitrate tetrahydrate (Fluka, Buchs, Switzerland, 97%), were dissolved in deionized water and complexed [23] with citric acid (Gram-mol, Zagreb, Croatia, 99.5%), while pH was adjusted to 7 with ammonia (Kemika, Zagreb, Croatia, 25%). Samples were spray-dried in a Büchi 290 apparatus (Büchi Labortechik, Flawil, Switzerland) in a co-current stream with a liquid feed rate of 160 mL $h^{-1}$, a 1.4 mm nozzle and an inlet air temperature of 190 °C. The atomizing gas flow rate through the nozzle was set using a rotameter; a reading of 65 mm corresponds to 819 NL $h^{-1}$, according to the manufacturer's calibration table. Thermal treatment was accomplished in a muffle furnace at 700 °C for 4 h. The removal of secondary phases was accomplished by washing the samples with concentrated HCl (Kemika, Zagreb, Croatia, 37%) heated to 70 °C, using 70 mg of pigment in 70 $cm^3$ of the solution. The suspensions were stirred for 3 h at elevated temperature and then centrifuged. The obtained samples were rinsed 4 times with demineralized water and finally dried at 60 °C overnight.

The thermal evolution of samples was characterized utilizing a NETZSCH STA-449C simultaneous differential thermal and thermogravimetric analyzer (Netzsch, Selb, Germany) with a sample mass of 50 mg, α-alumina crucibles and reference material, temperature rate of 10 °C $min^{-1}$, and flowing air rate of 30 $cm^3$ $min^{-1}$. Crystal phases were determined

via X-ray diffraction using Shimadzu XRD 6000 (Shimadzu, Tokyo, Japan) with Cu Kα radiation, a 0.02 step and 0.6 s retention time. Crystal lattice parameters *a* and *c* were calculated through the Unitcell program [24]. Microstructure was characterized using a Vega 3 scanning electron microscope (Tescan, Brno, Czech Republic) operating at 10 kV. Energy-dispersive X-ray spectroscopy (EDS) was performed using a Bruker Quantax system (Bruker, Billerica, MA, USA) integrated into the aforementioned SEM. All analyses were carried out under identical acquisition conditions to ensure comparability, using an accelerating voltage of 10 kV, a working distance of 20 mm, and a beam intensity of 15. Quantitative data were obtained using the built-in database, and background subtraction and peak integration were accomplished using the device software. UV-Vis reflectance spectra and CIE L*a*b* color parameters were obtained utilizing Ocean Insight QE Pro High-Performance Spectrometer (Ocean Optics, Orlando, FL, USA).

## 3. Results and Discussion

The spray-dried samples were first subjected to heat treatment at 700 °C for 4 h, resulting in completely X-ray amorphous fine powders. The pure sample appeared white, while the doped samples were brown.

DTA and TGA curves of the investigated samples are given in Figure 1. The endothermic peak found between room temperature and ~150 °C, accompanied by ~1.5% mass loss, is due to the release of water adsorbed during the storage of the calcined samples [7]. An additional broad peak, also accompanied by mass loss, can be observed roughly between 200 and 600 °C. Since the sample was calcined at 700 °C for 4 h, the presence of organic residues is highly unlikely. Therefore, this peak and mass loss are attributed to residual char oxidation.

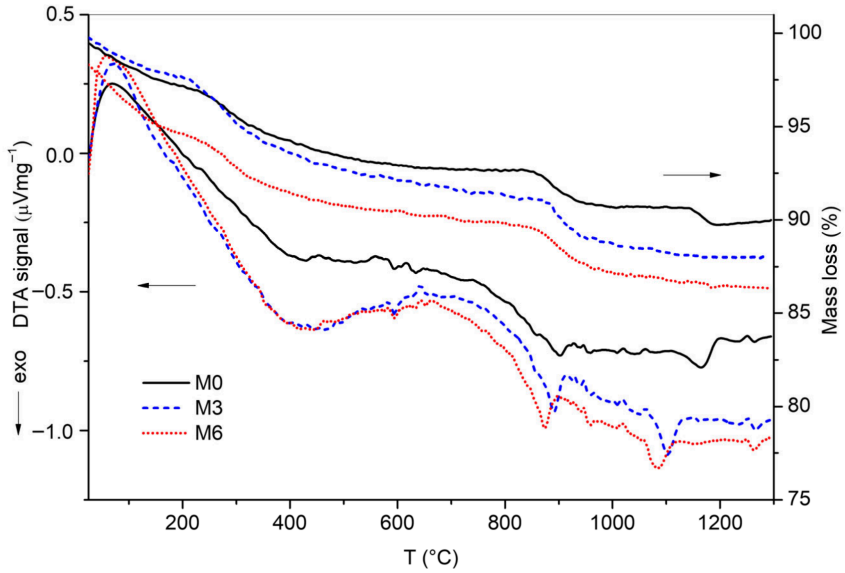


**Figure 1.** DTA and TGA curves of samples M0, M3 and M6 calcined at 700 °C for 4 h.

Two major peaks can be observed in the DTA curve. The first one is due to γ-alumina crystallization, with peak maxima at 902, 892 and 875 °C for samples M0, M3 and M6, respectively. The second is due to the γ- to α-alumina phase transformation, with maxima at 1166 (M0), 1104 (M3) and 1085 °C (M6) [11]. A decrease in the γ-alumina crystallization temperature, as well as the γ- to α-alumina transformation temperature with manganese loading, indicates at least the partial entry of manganese into the alumina crystal lattice [25]. The decrease in temperature required for the development of the α-alumina phase in the presence of manganese doping was also noted by Lopez-Navarrete and Ocana [7], who

considered a certain catalytic effect of Mn doping on α-alumina formation. Jähnichen et al. [26] also noted that manganese assisted the conversion to α-alumina at low temperatures, arguing that the first formed manganese-rich corundum-type domains act as seeding crystals for alumina.

TGA curves show mass loss in several intervals. In the range up to 100 °C, losses of physiosorbed water occur, while in the range between 100 and 600 °C, organic residues are burned off [22]. The TGA curves of all samples also show mass loss roughly between 850 and 1000 °C. The pure sample curve shows additional mass loss roughly between 1150 and 1200 °C, while the curves of the doped samples show continuous mass loss in the high-temperature range. Mass losses indeed coincide roughly with the peaks, but the process of γ-alumina crystallization and the γ- to α-alumina transformation should not cause mass loss. Upon a closer look, it becomes obvious that the mass loss occurs after the appearance of an exothermic peak. Therefore, these losses are attributed to the oxidation of char trapped in the pores, which comes into contact with oxygen through microstructural changes accompanying crystallization and phase transformation [27]. Char is a carbon-rich residue that remains after the incomplete combustion or pyrolysis of organics, in this case citric acid. In the course of thermal treatment prior to thermal analysis, the decarboxylation of organic carboxyl groups occurs and is accompanied by the release of carbon dioxide, carbon monoxide and water vapor [28]. The continuous polymer network collapses into an amorphous matrix, while residual carbon pyrolyzes into char [29]. Lopez-Navarrete and Ocana [7] attributed a small mass loss detected in a very similar system around 1000 °C to the release of residual OH groups, which is also a plausible explanation. Total mass losses are 10.1, 12.0 and 13.6% for samples M0, M3 and M6, respectively. The majority of mass loss is associated with physiosorbed water and organic residue, roughly 7.3, 8.9 and 10.4% for samples M0, M3 and M6, respectively. The additional mass losses, occurring in two stages (2.1% and 0.6%) for sample M0 and in a single stage (3.1% and 3.3%) for samples M3 and M6, could be attributed to the oxidation of residual char trapped in the pores [29], which became available due to structural transformations. It should be noted that manganese oxides undergo a progressive, stepwise reduction in oxygen content as the temperature increases during thermal analysis, which can also contribute to weight loss. As can be seen in Figure 1, the difference in mass loss between samples M3 and M6 is mainly in the initial water content, probably because the M6 storage time after heat treatment is slightly longer. However, it is obvious that the doped samples lose slightly more mass than the pure one.

Subsequently, the samples underwent thermal treatment to determine the optimal calcination temperatures required to induce crystallization. The XRD patterns of the investigated samples thermally treated at various temperatures are given in Figure 2a–c. As can be observed, the pure sample heat-treated at 1000 °C contains two phases, γ-alumina, γ-$Al_2O_3$ (ICDD PDF No. 10-425), and α-alumina, α-$Al_2O_3$ (ICDD PDF No. 10-173). In other words, in this sample, the γ- to α-alumina phase transformation was not completed after thermal treatment at 1000 °C for 4 h. Although the results of DTA/TGA analysis indicate that the transformation takes place at a higher temperature (with the greatest rate at 1166 °C), it is obvious that the process commences at a far lower temperature, even if one takes into consideration the possible discrepancy between the temperatures measured in the DTA/TGA apparatus and muffle furnace. Notably, DTA/TGA is precisely calibrated and has better temperature regulation, and temperature is measured by a thermocouple in direct contact with the sample. On the other hand, in the kiln, thermal regulation is poorer, chamber temperature is less uniform, and the thermocouple is located at a certain distance from sample. This can lead to deviations of up to several tens of °C. However, at this temperature, the process is so slow that 4 h of thermal treatment is not enough to achieve a complete transformation. On the other hand, heat treatment at 1100 °C for 4 h leads to

the complete transformation of γ- to α-alumina, and thus, in this sample, α-alumina is the single crystal phase, i.e., there are no detectable impurities, at least not with a proportion greater than the XRD detection limit (at least 1%). The sample treated at 1200 °C for 4 h shows no notable changes. The relatively narrow XRD peaks of α-alumina in all samples indicate a high degree of crystallinity.

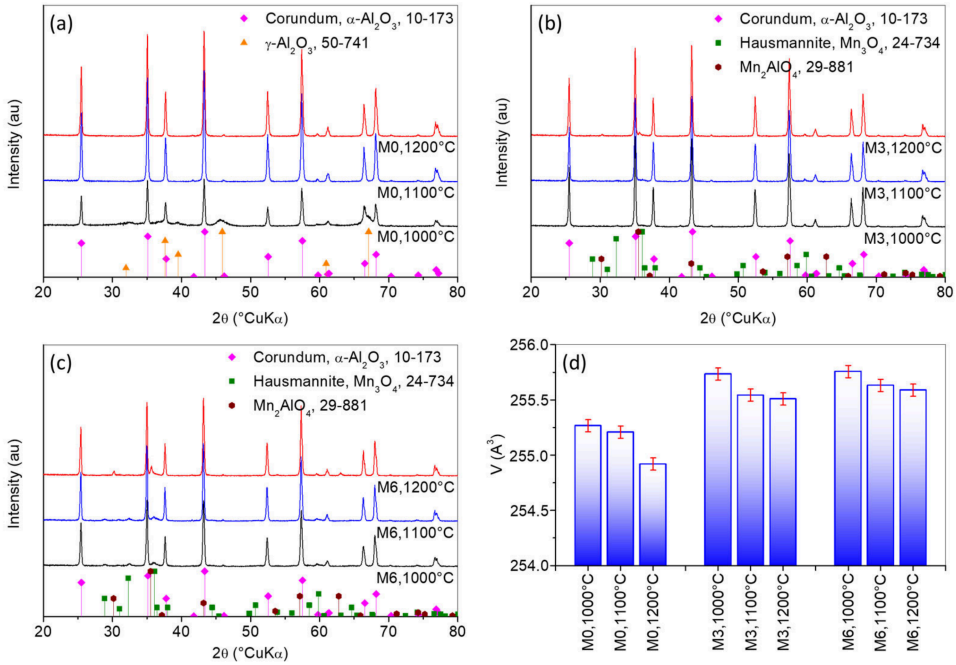


**Figure 2.** XRD patterns of samples (**a**) M0, (**b**) M3 and (**c**) M6 thermally treated at 1000, 1100 and 1200 °C for 4 h. (**d**) Unit cell volume of α-alumina for samples M0, M3 and M6 thermally treated at 1000, 1100 and 1200 °C for 4 h.

In the XRD pattern of sample M3 heat-treated at 1000 °C, the peaks of α-alumina and faint peaks of hausmannite, $Mn_3O_4$ (ICDD PDF No. 24-734), could be observed, i.e., doping the sample with manganese caused the appearance of a secondary phase. Although they are of very low intensity and broad, in the XRD pattern of sample M3, two of the strongest hausmannite peaks (211 and 103) at 36.08 and 32.32° 2θ are observable. While the secondary phase may be advantageous for suppressing grain growth and enabling better mechanical properties, when it comes to optical properties, a secondary phase can impair them [30]. In contrast to the undoped sample, there are no peaks corresponding to γ-alumina. It is obvious that a considerable shift in the γ- to α-alumina phase transition towards a lower temperature (greatest rate at 1104 °C) enabled the completion of this transformation already after 4 h treatment at 1000 °C. Heat treatment at 1100 °C does not lead to notable changes in the pattern's appearance. However, the XRD pattern of the sample treated at 1200 °C indicates the disappearance of hausmannite and the appearance of manganese aluminate, $Mn_2AlO_4$ (ICDD PDF No. 29-881). Again, only two peaks of low intensity, 311 at 35.52 and 220 at 30.17° 2θ, can be observed. The presence of hausmannite and aluminate phases points to limited manganese solubility in alumina. In the literature, the limited solubility of manganese in alumina is attributed to the mismatch of ionic radii and charge imbalance between guest and host ions. Due to differences in ionic radii, significant lattice strain appears, while due to the charge imbalance, oxygen vacancies have to be created, which is thermodynamically unfavorable [1,4]. If present above the solubility limit, manganese forms an additional crystalline phase [31].

The XRD patterns of sample M6 are very similar to those of sample M3. Here, (311 and 220) hausmannite peaks can clearly be observed. Certain sharpening of a man-

ganese spinel peak at 35.5° 2θ could be observed in the XRD patterns of samples heat-treated at 1000 and 1100 °C. The appearance of manganese aluminate is often recorded in Mn-doped alumina [1,8,10]. Both doped samples have approximately the same phase crystallization path. Hausmannite appears next to α-alumina at 1000 °C and then disappears at higher temperatures, while manganese aluminate appears. It is therefore reasonable to assume that hausmannite reacts with alumina in some reactive form [32], most probably with the traces of γ-alumina invisible to XRD. One reason why the γ-alumina phase can be effectively undetectable to standard XRD could be its disordered structure and nanocrystalline size [33].

The crystal lattice parameters *a* and *c*, as well as cell volume, *V*, of α-alumina were calculated through the Unitcell program [24]. The obtained lattice parameters for the pure sample thermally treated at 1000 °C for 4 h were *a* = 4.7622(2) and *c* = 12.9971(2) Å, which is slightly greater than those from ICDD PDF No. 10-173 data (*a* = 4.7591 and *c* = 12.9894 Å). Thermal treatment at 1200 °C for 4 h pushes these values closer to the literature data (*a* = 4.7591(2) and *c* = 12.9966(2) Å). Doped samples show slightly greater lattice parameters, e.g., after 1200 °C for 4 h, values are *a* = 4.7641(2) and *c* = 12.9990(2) Å for sample M3 and *a* = 4.7646(2) and *c* = 13.0004(2) Å for sample M6. According to Farag et al. [25], the *a*-axis lattice parameter of Mn-doped $Al_2O_3$ exhibits only minor changes with increasing Mn content, whereas the *c*-axis shows more significant variations. Therefore, the cell volumes of all investigated samples, which proved to be the most suitable for comparison, are shown in Figure 2d.

Figure 2d clearly shows that doping leads to an expansion of the α-alumina unit cell. Regardless of the thermal treatment temperature, the unit cell volume of the doped samples is larger than that of the pure sample. This is expected since Mn(II) and Mn(III) cations have a larger radius than Al(III), which they should replace in the α-alumina crystal lattice. According to the literature [34], the ionic radii of Mn(II) and Mn(III) in octahedral coordination are 0.67 and 0.58 Å, respectively, while the ionic radius of Al(III) in the same coordination is 0.54 Å. On the other hand, Mn(IV) in octahedral coordination has an ionic radius of 0.53 Å, so the replacement of Al with Mn(IV) would not cause significant changes in the cell volume. Therefore, unit cell expansion can be considered evidence of manganese incorporation into the crystalline structure of α-alumina, i.e., the formation of solid solution.

A certain decrease in cell volume with an increase in annealing temperature can be observed for all three samples. In the literature, such a phenomenon is attributed primarily to the elimination of defects and structural relaxation [35–37]. The crystal lattice of the phase obtained by annealing at a low temperature is characterized by a high density of point defects (vacancies or interstitials) and microstrain, resulting in larger lattice parameters. With an increase in thermal treatment temperature, additional thermal energy is provided, enabling a more perfect atomic arrangement and yielding lattice contraction [37] towards its dimensions as reported in ICDD PDF No. 10-173. The interaction of dangling bonds (unsatisfied valences on immobilized atoms) present on the surface with oxygen ions from the environment is also mentioned as a possible reason for cell contraction [35]. Lopez-Navarrete and Ocana [7] offer another explanation of the cell shrinkage seen with annealing temperature for the particular case of Mn-doped alumina. Based on the fact that a partial reduction of Mn(III) to Mn(II) occurs at higher temperatures [38], they assume that this reduces the amount of Mn available for the formation of Mn:$Al_2O_3$ solid solution. The consequence is the contraction of the unit cell of the α-alumina solid solution. In the present case, although Mn(II) appears in the system, which is evidenced by the appearance of manganese aluminate, the source of this Mn(II) is probably hausmannite, according to the crystallization path of previously discussed phases. Also, as can be observed in Figure 2d, the decrease in cell volume with temperature also occurs for the pure sample.

Therefore, we are more inclined to attribute this phenomenon to the elimination of defects and structural relaxation. Comparing the three samples, it is evident that cell shrinkage is not an overemphasized effect, and total expansion with dopant entrance is still present.

In Figure 3a–e, the microstructure of prepared samples is displayed. The microstructure is rather similar for all samples, regardless of doping or thermal treatment temperature. All samples consist of particles of irregular shapes and sizes. These particles are basically agglomerates with irregular shapes consisting of much smaller clusters. Commonly, almost perfect spheres are formed via spray drying, which was not the case here. Irregularly coccoid particles with a lot of protrusions were formed instead [23]. This could be attributed to the presence of citric acid as a chelating agent that, upon heating and water evaporation, forms a highly viscous, polymer-like network which hinders the formation of spheres. Later, after thermal treatment, such morphology turned into irregularly shaped agglomerates, which are far from the ideal pigment morphology, which should be smooth monodispersed spherical particles, ensuring fluidity and good dispersion in the course of application.

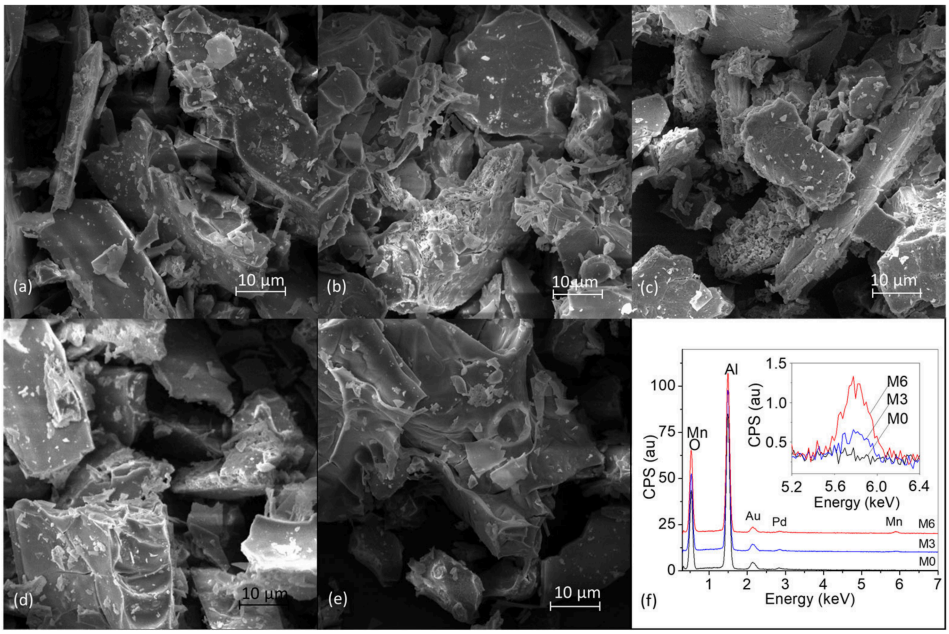


**Figure 3.** SEM micrograph of (**a**) sample M3 thermally treated at 1000 °C for 4 h, (**b**) sample M3 thermally treated at 1100 °C for 4 h, (**c**) sample M3 thermally treated at 1200 °C for 4 h, (**d**) sample M0 thermally treated at 1000 °C for 4 h, and (**e**) sample M6 thermally treated at 1000 °C for 4 h. (**f**) EDS spectra of samples M3 and M6 thermally treated at 1000 for 4 h.

The EDS spectra of samples thermally treated at 1000 °C are displayed in Figure 3f. Aluminum and oxygen are the predominant elements, although a weak manganese signal can also be detected (inset of Figure 3f). On the basis of the EDS spectra, the chemical composition of the samples was determined and is given in Table 1. As can be observed, sample M3 contains 1.2 at. % of Mn. Recalculation to cation percent yields $1.2/(43.4 + 1.2)\cdot 100 = 2.7\%$. Considering the limitations of the EDS method, this is fairly close to the nominal Mn percent of 0.03. Sample M6 contains 2.7 at. % of Mn, which corresponds to a cation percent of 6.0%, which is equal to the nominal composition. It should be noted that EDS analysis confirms the presence and approximate amount of Mn, but it does not provide direct evidence of its incorporation into the crystal lattice; rather, it supports compositional consistency and, together with the XRD results, is consistent with Mn incorporation into the lattice.

**Table 1.** Chemical composition of samples thermally treated at 1000 °C for 4 h, as well as samples washed with HCl, obtained from EDS spectra.

| Sample | Al (at. %) | O (at. %) | Mn (at. %) |
|---|---|---|---|
| M0 | 41.7 ± 1.6 | 58.3 ± 1.1 | - |
| M3 | 43.4 ± 1.4 | 55.4 ± 1.0 | 1.2 ± 0.2 |
| M6 | 42.6 ± 1.6 | 54.7 ± 1 | 2.7 ± 0.3 |
| M3 washed | 38.0 ± 1.3 | 61.4 ± 1.2 | 0.6 ± 0.2 |
| M6 washed | 45.8 ± 1.4 | 53.1 ± 1.3 | 1.1 ± 0.2 |

The prepared doped samples after thermal treatment at 1000 °C for 4 h were brown, with sample M6 being slightly darker than M3, while the pure sample was white. The brown color observed in the doped samples heat-treated at 1000 °C is attributed to the presence of hausmannite, which is reported to have a brownish-black to grayish color [39]. The color of samples thermally treated at 1100 and 1200 °C for 4 h was brick red. In order to remove hausmannite, the samples thermally treated at 1000 °C for 4 h were leached in hot concentrated hydrochloric acid in which hausmannite is soluble [6]. The treatment was successful, as immediately indicated by the appearance of a pink color. According to Lopez-Navarette et al. [7], the pink color in this system is due to the presence of Mn(III) ions within the α-alumina lattice. As can be observed in Figure 4, the microstructure of prepared samples did not change significantly with washing and can again be described as agglomerates of irregular shapes and sizes.

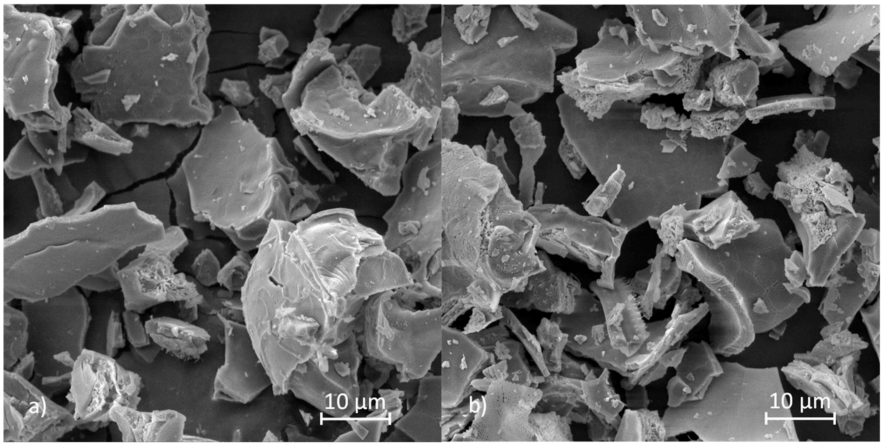


**Figure 4.** SEM micrograph of (**a**) washed sample M3 thermally treated at 1000 °C for 4 h and (**b**) washed sample M3 thermally treated at 1100 °C for 4 h.

The XRD patterns of washed samples M3 and M6 thermally treated at 1000 °C for 4 h, confirming the elimination of hausmannite, are given in Figure 5a, while the EDS spectra of the same samples are given in Figure 5b. As can be observed in Figure 5a, the weak hausmannite diffraction peaks disappeared from the XRD patterns after acidic washing. This is accompanied by a decrease in manganese content, as observed in the EDS spectra (Figure 5b). The chemical composition of the doped samples after washing is given in Table 1. The quantity of Mn in samples M3 and M6 is reduced to 0.6 and 1.1 at. %, respectively (corresponding to cation percents 1.6 and 2.3%).

The remaining manganese is suggested to be incorporated into the Mn:$Al_2O_3$ solid solution, as indicated by the absence of secondary phases and the observed lattice expansion, in agreement with the XRD analysis. The appearance of a pink coloration is consistent with this interpretation. This is beyond the expectations of this study, but there are numerous

references in the literature indicating that the solubility limit of manganese in alumina is low [1,30,31,40].

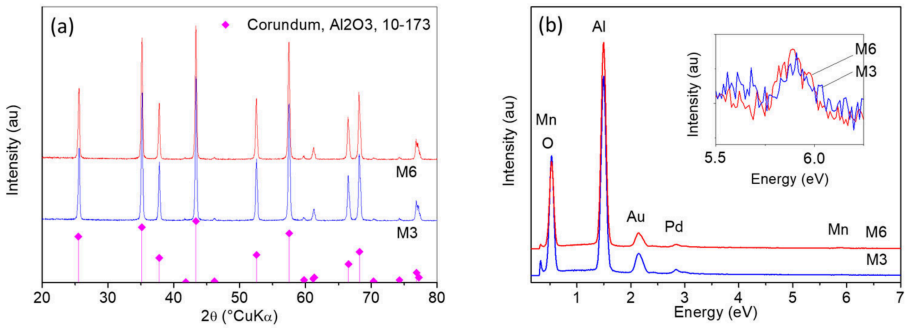


**Figure 5.** (**a**) XRD patterns and (**b**) EDS spectra of washed samples M3 and M6.

Therefore, manganese replaces aluminum in the host α-alumina lattice, but a discrepancy exists between the nominal composition and the amount of manganese entering the α-alumina lattice due to the appearance of secondary manganese phases. Such a discrepancy has been noted in the literature [25,31]. Our synthesis strategy was based on the preparation of an amorphous precursor with a homogeneous distribution of manganese. Homogeneous distribution should enable short diffusion paths in the course of the crystallization process, leading to greater dopant solubility. Such a strategy is typical for, for example, sol–gel synthesis or colloidal precipitation [41]. A possible improvement in manganese incorporation could be achieved by using nanosized precursor particles. Dopants often segregate to grain boundaries, and since nanoparticles have a greater grain boundary volume, they enable the hosting of a higher amount of dopant [42].

The reflectance spectra of samples thermally treated at 1000 °C are given in Figure 6. The pure sample exhibits very good reflectance in the visible range, while the reflectance of the doped samples can be considered fair, likely due to the presence of hausmannite. As expected, the sample with a higher manganese content and a greater amount of hausmannite shows slightly reduced reflectance compared to the sample with a lower manganese load. The spectra of doped samples show absorbance in the region between 400 and 600 nm, with it being the greatest at around 530 nm. This band is interpreted as a consequence of $^5E_g \rightarrow {}^5T_2$ transitions in Mn(III) ions in octahedral positions in the α-alumina lattice [43]. The broadness of this band is attributed to the Jahn–Teller splitting of $^5E_g$ and $^5T_2$ transitions. Nagashima et al. [14] reported a transmittance curve showing a drop at wavelengths at ~500 ± 50 nm, which they ascribed to manganese doping. The wavelength of 530 nm corresponds to the green color. Consequently, the pigment shows the color complementary to green, i.e., pink. Washing removes most of the hausmannite, resulting in improved reflectance in the visible range for the washed samples compared to the as-prepared ones. However, although hausmannite is not detectable by XRD, possibly due to its low concentration, its presence can still be inferred from the absorbance spectra. This inference is further supported by the observation that the pigment with higher manganese content exhibits slightly lower reflectance.

Color evaluation was done using Comission Internationale de l'Eclairage (CIE) L*a*b* chromatic coordinates, where L* is color lightness (L* = 0 for black and L* = 100 for white), a* is the green (−)/red (+) axis, and b* is the blue (−)/yellow (+) axis. The chromatic coordinates (L*, a* and b*) of the prepared samples are given in Table 2. As stated before, prepared samples after acid washing appear pink. Differences in manganese loading did not cause great changes in the L*a*b* parameters. A certain increase in lightness and increase in the red and yellow components with manganese loading can be observed. An increase in red is expected from these results since it is consistent with the slightly more intense pink in

the M6 sample. The increase in lightness and the yellow component are mutually consistent and probably originate from fluorescence. It is well known that $Mn^{2+}$-containing materials exhibit photoluminescence in the wavelength range corresponding to the yellow color [44]. In comparison with literature data [9], the prepared pigment is very bright but pale, providing a pastel warm pink color.

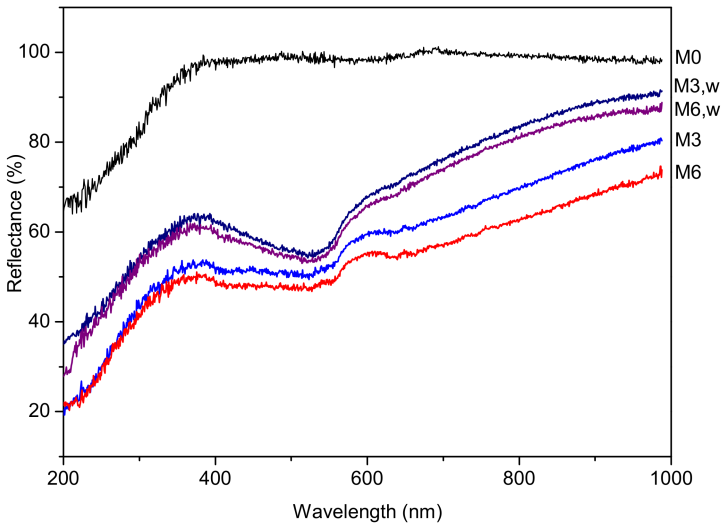


**Figure 6.** UV-Vis DRS spectra of samples heat-treated at 1000 °C and washed with HCl.

**Table 2.** Chromatic coordinates of samples M3 and M6 thermally treated at 1000 °C for 4 h and washed with concentrated HCl.

| Sample | L | a | b |
|---|---|---|---|
| M3 | 80.691 | 8.293 | 4.377 |
| M6 | 81.967 | 8.552 | 5.002 |

## 4. Conclusions

Samples of alumina where 3 and 6 mol. % of aluminum were substituted with manganese were successfully prepared by the spray drying method. Manganese presence shifted the γ- to α-alumina phase transformation to lower temperatures. After thermal treatment at 1000 °C for 4 h, α-alumina was the dominant phase, accompanied by the appearance of hausmannite. The incorporation of manganese into the α-alumina crystal lattice was confirmed by unit cell expansion. Thermal treatment to higher temperatures resulted in the disappearance of hausmannite and the formation of manganese aluminate. The presence of dopant did not cause notable modifications of morphology. Upon washing the samples with a hot, concentrated HCl solution, a distinct pink coloration appeared. This treatment removed a significant portion of manganese-containing secondary phases, while the remaining manganese was predominantly associated with the α-alumina phase, as suggested by XRD analysis, resulting in a reduction in the total manganese content in the samples by at least half. Colorimetric analysis showed that the lightness, redness and yellowness of the prepared pigments increased with manganese loading.

**Author Contributions:** Conceptualization, S.K.; methodology, S.K., K.M. and A.P.; validation, K.M.; formal analysis, K.M. and A.P.; investigation, S.K., K.M. and A.P.; resources, S.K.; data curation, S.K. and K.M.; writing—S.K.; writing—review and editing, S.K. and K.M.; visualization, S.K.; supervision, S.K.; project administration, S.K.; funding acquisition, S.K. Author A.P. passed away prior to the publication of this manuscript. All other authors have read and agreed to the published version of this manuscript.

**Funding:** This research was conducted within the framework of the project HEMCAT financed by the European Union's—NextGenerationEU fund from the source 581—The recovery and resilience mechanism in the frame of Programme financing of public higher education institutions and public scientific institutes.

**Data Availability Statement:** The original contributions presented in this study are included in the article. Further inquiries can be directed to the corresponding author.

**Acknowledgments:** The support of the University of Zagreb, Faculty of Chemical Engineering and Technology, is gratefully acknowledged. During the preparation of this work, the authors used ChatGPT (OpenAI, based on GPT-5 architecture, https://chat.openai.com/, accessed on 6 March 2025) in order to check grammar and improve stylistic clarity in some sections of the manuscript. After using this tool, the authors reviewed and edited the content as needed and take full responsibility for the content of the publication.

**Conflicts of Interest:** The authors declare no conflicts of interest.

## References

1. Dhuban, S.B.; Ramesh, S.; Tan, C.Y.; Wong, Y.H.; Johnson Alengaram, U.; Ramesh, S.; Teng, W.D.; Tarlochan, F.; Sutharsini, U. Sintering behaviour and properties of manganese-doped alumina. *Ceram. Int.* **2019**, *45*, 7049–7054. [CrossRef]
2. Kurajica, S.; Mali, G.; Mandić, V.; Simčić, I.; Matijašić, G.; Mužina, K. Tailoring microstructural, textural and thermal properties of transition-alumina by modifying aluminium sec-butoxide with ethyl acetoacetate within a sol-gel synthesis. *J. Phys. Chem. Solids* **2021**, *148*, 109783. [CrossRef]
3. Ricceri, R.; Ardizzone, S.; Baldi, G.; Matteazzi, P. Ceramic pigments obtained by sol-gel techniques and by mechanochemical insertion of color centers in $Al_2O_3$ host matrix. *J. Eur. Ceram. Soc.* **2002**, *22*, 629–637. [CrossRef]
4. Lennox, J.; Pepper, R.; Martens, W.; Gray, V.; Alarco, J.; MacLeod, J.; Couperthwaite, S. Connection between alumina doping methodology and performance: A review. *Ceram. Int.* **2026**, *52*, 18024–18049. [CrossRef]
5. Hara, H.; Younes, R.; Bradai, M.A.; Alymov, M. Characterization of manganese and cobalt doping effects in sol-gel synthesized alumina powder. *Chem. Afr.* **2025**, *8*, 5589–5603. [CrossRef]
6. Lopez-Navarrete, E.; Caballero, A.; Gonzalez-Elipe, A.R.; Ocana, M. Chemical state and distribution of Mn ions in Mn-doped $\alpha$-$Al_2O_3$ solid solutions prepared in the absence and the presence of fluxes. *J. Eur. Ceram. Soc.* **2004**, *24*, 3057–3062. [CrossRef]
7. Lopez-Navarrete, E.; Ocana, M. Aerosol-derived Mn-doped $Al_2O_3$ pink pigments prepared in the absence of fluxes. *Dye. Pigment.* **2004**, *61*, 279–286. [CrossRef]
8. Wang, S.; Yang, J.; Ouyang, X.; Han, D. Synthesis and Properties of Mn-doped Alumina Red Pigment Prepared by Low-temperature Combustion-Calcination Process. *Adv. Mater. Res.* **2011**, *250–253*, 769–772. [CrossRef]
9. Cruzeiro, M.T.R.; Moraes, F.A.; Kaizer, M.R.; Moreira, M.L.; Zhang, Y.; Moraes, R.R.; Cava, S.S. Functionalized pink $Al_2O_3$:Mn pigments applied in prosthetic dentistry. *Prosthet. Dent.* **2017**, *118*, 771–777. [CrossRef]
10. Zvonarev, S.V.; Frolov, E.I.; Chesnokov, K.Y.; Smirnov, N.O.; Pankov, V.A.; Churkin, V.Y. Luminescent properties of alumina ceramics doped with manganese and Magnesium. *Opt. Mater.* **2019**, *91*, 349–354. [CrossRef]
11. Hernandez, T.; Bautista, C.; Martin, P. Synthesis and thermal evolution of Mn-doped alumina nanoparticles by homogeneous precipitation with urea. *Mat. Chem. Phys.* **2005**, *92*, 366–372. [CrossRef]
12. Ianoș, R.; Muntean, E.; Băbuță, R.; Lazău, R.; Păcurariu, C.; Bandas, C. Combustion synthesis of pink chromium-doped alumina with excellent near-infrared reflective properties. *Ceram. Int.* **2017**, *43*, 2568–2572. [CrossRef]
13. Drdlikova, K.; Drdlika, D.; Hadraba, H.; Klement, R.; Maca, K. Optical and mechanical properties of Mn-doped transparent alumina and their comparison with selected rare earth and transient metal doped aluminas. *J. Eur. Ceram. Soc.* **2020**, *40*, 4894–4900. [CrossRef]
14. Nagashima, M.; Motoike, K.; Hayakawa, M. Fabrication and optical characterization of high-density $Al_2O_3$ doped with slight MnO dopant. *J. Ceram. Soc. Jpn.* **2008**, *116*, 645–648. [CrossRef]
15. Kannan, T.S.; Panda, P.K.; Jaleel, V.A. Preparation of Pure $Al_2O_3$ and Alumina Doped with Oxides of Magnesium, Chromium and Manganese by Hydrothermal Oxidation of Aluminium Metal. *Trans. Indian Ceram. Soc.* **1999**, *58*, 1–4. [CrossRef]
16. Crisan, M.; Raileanu, M.; Preda, S.; Zaharescu, M.; Valean, A.M.; Popovici, E.J.; Teodorescu, V.S.; Matejc, V.; Mrazek, J. Manganese doped sol-gel materials with catalytic Properties. *J. Optoelectron. Adv. Mater.* **2006**, *8*, 815–819.
17. Gholizadeh, Z.; Aliannezhadi, M. Tailoring the morphology and optical properties of alumina nanostructures by carbon quantum dot modification for enhanced heavy metal adsorption. *Microsyst. Nanoeng.* **2026**, *12*, 80. [CrossRef]
18. Bertrand, G.; Filiatre, C.; Mahdjoub, H.; Foissy, A.; Coddet, C. Influence of slurry characteristics on the morphology of spray-dried alumina powders. *J. Eur. Ceram. Soc.* **2003**, *23*, 263–271. [CrossRef]

19. Zhang, S.; Gong, G.; Wang, H.; Chen, S.; Wang, J.; Qi, J. Advances and challenges of the spray drying technology: Towards accurately constructing inorganic multi-functional materials and related applications. *Sustain. Mater. Technol.* **2025**, *43*, e01250. [CrossRef]
20. Stunda-Zujeva, A.; Irbe, Z.; Berzina-Cimdina, L. Controlling the morphology of ceramic and composite powders obtained via spray drying—A review. *Ceram. Int.* **2017**, *43*, 11543–11551. [CrossRef]
21. Nandiyanto, A.B.D.; Okuyama, K. Progress in developing spray-drying methods for the production of controlled morphology particles: From the nanometer to submicrometer size ranges. *Adv. Powder Technol.* **2011**, *22*, 1–19. [CrossRef]
22. Stoyanova Lyubenova, T.; Matteucci, F.; Costa, A.L.; Dondi, M.; Ocaña, M.; Carda, J. Synthesis of Cr-doped $CaTiSiO_5$ ceramic pigments by spray drying. *Mat. Res. Bull.* **2009**, *44*, 918–924. [CrossRef]
23. Kurajica, S.; Mužina, K.; Petračić, A.; Teržan, J.; Car, F.; Likozar, B.; Miloš, K. Properties and catalytic activity of spray-dried alumina supported $MnO_x$ Catalysts. *J. Therm. Anal. Calorim.* **2025**, *150*, 923–935. [CrossRef]
24. Holland, T.J.B.; Redfern, S.A.T. UNITCELL: A nonlinear least-squares program for cell-parameter refinement implementing regression and deletion diagnostics. *J. Appl. Cryst.* **1997**, *30*, 84. [CrossRef]
25. Farag, I.S.A.; El-Rafaay, N.M. Study of dielectric properties of α-alumina doped with MnO, CdO and MoO. *Ind. J. Phys.* **2005**, *43*, 446–458.
26. Jähnichen, T.; Carstens, S.; Franz, M.; Laufer, O.; Wenzel, M.; Matysik, J.; Enke, D. Towards high surface area α $Al_2O_3$–Mn-assisted low temperature transformation. *Materials* **2023**, *16*, 3047. [CrossRef]
27. Kurajica, S.; Mužina, K.; Simčić, I.; Mandić, V. Thermal evolution of gels prepared by chelation of aluminum sec-butoxide with ethyl acetoacetate in various amounts. *J. Therm. Anal. Calorim.* **2023**, *148*, 1231–1239. [CrossRef]
28. Behera, P.S.; Bhattacharyya, S.; Sarkar, R. Effect of citrate to nitrate ratio on the sol-gel synthesis of nanosized α-$Al_2O_3$ powder. *Ceram. Int.* **2017**, *43*, 15221–15226. [CrossRef]
29. Sato, T.; Ikoma, S.; Ozawa, F. Thermal decomposition of aluminium hydroxycarboxylates—Lactate, citrate and tartrate. *J. Chem. Technol. Biotechnol.* **2007**, *33*, 415–420. [CrossRef]
30. Svoboda, J.; Drdlíková, K.; Drdlík, D.; Kroupa, A.; Michalička, J.; Maca, K. Doping of alumina ceramics by manganese—Thermodynamical and experimental approach. *Process. Appl. Ceram.* **2022**, *16*, 13–21. [CrossRef]
31. Mottye, J.; Ratzker, B.; Kalabukhov, S.; Favelukis, B.; Hayun, S.; Frage, N. Effect of Mn doping on the densification and properties of transparent alumina by high-pressure spark plasma sintering. *Ceram. Int.* **2023**, *49*, 28369–28375. [CrossRef]
32. Navarro, R.C.; de Avillez, R.R.; Goes, T.F.; Gomes, A. Low temperature thermal and volumetric behavior of $MnAl_2O_4$ spinel. *J. Mater. Res. Technol.* **2020**, *9*, 4194–4205. [CrossRef]
33. Xu, S.; Jaegers, N.R.; Hu, W.; Kwak, J.H.; Bao, X.; Sun, J.; Wang, Y.; Hu, J.Z. High-field one-dimensional and two-dimensional $^{27}$Al magic-angle spinning nuclear magnetic resonance study of θ-, δ-, and γ-$Al_2O_3$ dominated aluminum oxides: Toward understanding the Al sites in γ-$Al_2O_3$. *ACS Omega* **2021**, *6*, 4090–4099. [CrossRef]
34. Available online: http://abulafia.mt.ic.ac.uk/shannon/ptable.php (accessed on 6 March 2025).
35. Malevu, T.D.; Ocaya, R.O. Effect of Annealing Temperature on Structural, Morphology and Optical Properties of ZnO Nano-Needles Prepared by Zinc-Air Cell System Method. *Int. J. Electrochem. Sci.* **2015**, *10*, 1752–1761. [CrossRef]
36. Teh, G.B.; Wong, Y.C.; Tilley, R.D. Effect of annealing temperature on the structural, photoluminescence and magnetic properties of sol-gel derived Magnetoplumbite-type (M-type) hexagonal strontium ferrite. *J. Magn. Magn. Mater.* **2011**, *323*, 2318–2322. [CrossRef]
37. Samavati, A.; Othaman, Z.; Ghoshal, S.K.; Mustafa, M.K. The influence of growth temperature on structural and optical properties of sputtered ZnO QDs embedded in $SiO_2$ matrix. *Superlattices Microstruct.* **2015**, *86*, 134–142. [CrossRef]
38. Al Sagheer, F.A.; Hasan, M.A.; Pasupuleti, L.; Kaki, M.I. Low temperature synthesis of hausmannite $Mn_3O_4$. *J. Mat. Sci. Lett.* **1999**, *18*, 209–211. [CrossRef]
39. Available online: https://webmineral.com/data/Hausmannite.shtml (accessed on 6 March 2025).
40. Farina, A.B.; Neto, F.B. Thermodynamic modelling of an $Al_2O_3$@MnO system using the ionic model. *Calphad* **2009**, *33*, 711–718. [CrossRef]
41. Kurajica, S.; Tkalčec, E.; Mandic, V.; Schmauch, J. Mullite crystallization kinetics of lanthanum doped sol–gel derived precursors. *J. Eur. Ceram. Soc.* **2011**, *31*, 377–383. [CrossRef]
42. Futazuka, T.; Ishikawa, R.; Shibata, N.; Ikuhara, Y. Grain boundary structural transformation induced by co-segregation of aliovalent dopants. *Nat. Commun.* **2022**, *13*, 5299. [CrossRef] [PubMed]

43. Khomenko, O.V.; Berezovskaya, I.V.; Stoyanova, I.V.; Efryushina, N.P.; Dotsenko, V.P. Synthesis and Luminescence Study of Mn-doped Nanosized $Al_2O_3$, NAP-2018. In *Proceedings of the IEEE 8th International Conference on Nanomaterials: Applications & Properties, Zatoka, Ukraine, 9–14 September 2018*; IEEE: Piscataway, NJ, USA, 2018; pp. 1–4. [CrossRef]
44. El Mir, L.; Omri, K. Effect of manganese content on yellow luminescence properties of zinc silicate nanoparticles enriched silica matrix. *J. Lumin.* **2018**, *203*, 336–340. [CrossRef]

**Disclaimer/Publisher's Note:** The statements, opinions and data contained in all publications are solely those of the individual author(s) and contributor(s) and not of MDPI and/or the editor(s). MDPI and/or the editor(s) disclaim responsibility for any injury to people or property resulting from any ideas, methods, instructions or products referred to in the content.